Applied Catalysis B: Environmental 166–167 (2015) 211–216

Contents lists available at ScienceDirect

Applied Catalysis B: Environmental

journal homepage: www.elsevier.com/locate/apcatb

NO_x conversion properties of a novel material: Iron nanoparticles stabilized in carbon

Martin Busch[a,b,c], Alexander Kompch[a,c], Samer Suleiman[a,c], Christian Notthoff[a,c], Ulf Bergmann[b,c], Ralf Theissmann[d], Burak Atakan[b,c], Markus Winterer[a,c,*]

[a] Nanoparticle Process Technology, Faculty of Engineering, University of Duisburg-Essen, Lotharstrasse 1, 47057 Duisburg, Germany
[b] Thermodynamics, Faculty of Engineering, University of Duisburg-Essen, 47057 Duisburg, Germany
[c] Center for Nanointegration Duisburg-Essen, CENIDE, Duisburg, 47057 Duisburg, Germany
[d] Research Services/Analytical Intelligence, Kronos International, Inc., Peschstrasse 5, 51373 Leverkusen, Germany

ARTICLE INFO

Article history:
Received 28 April 2014
Received in revised form 2 November 2014
Accepted 8 November 2014
Available online 15 November 2014

Keywords:
Iron nanoparticles
Core–shell particles
Nitrogen oxide conversion
Carbon
Nitrogen oxide adsorption

ABSTRACT

Nitrogen oxides (NO_x) belong to the most common pollutants from combustion processes and are a major threat to human health. Carbon-based catalysts exhibit strong advantages for NO_x removal like low-toxic application and easy handling. However, gasification of the carbon matrix at elevated temperatures is still one of the greatest concerns. Hence, we have directed our focus on especially low temperature NO_x-removal using a novel material, iron nanoparticles stabilized in a carbon matrix (nano-Fe/C). The investigations included NO_2 uptake properties and catalytic conversion of NO_2 in recycle flow at 425 K and 328 K, scanning transmission electron microscopy and 77 K-N_2-adsorption.

Nano-Fe/C exhibits superior NO_x-removal properties compared with untreated or iron-infiltrated activated carbon or magnetite reference catalysts. No severe catalyst deactivation or catalyst aging at 425 K is observed. Even at 328 K nano-Fe/C still exhibits NO_2-conversion, although without converting the product NO. NO_2 adsorption at 297 K is suggested to occur in three stages with different kinetics: (1) NO_2 adsorption and reduction to NO, (2) physisorption on the oxidized catalyst surface and (3) saturation of the catalyst and diffusion into the substrate matrix. At 425 K, NO_2 is quickly reduced to NO and the resulting NO is further converted to N_2O. After complete consumption of NO, the residual NO_2 is also converted to N_2O. A possible reaction mechanism is suggested based on the conversion kinetics.

© 2014 Published by Elsevier B.V.

1. Introduction

Nitrogen oxides (NO_x) belong to the most common pollutants from combustion processes and are a threat to human health [1]. Their decomposition has been studied intensively during the last decades [2,3]. Common removal methods include three-way-catalysis, selective catalytic reactions using ammonia or hydrocarbons as co-reactant or – more recently – NO_x-storage-reduction [4–10]. Especially carbon-based catalysts have a long history in catalytic conversion of nitrogen oxides [11,12] since their advantages include low synthesis costs, non-toxic application as well as easy transportation and handling.

During the elucidation of the NO_x decomposition process a large number of various surface complexes are observed on carbonaceous materials [13,14], interpreted by different mechanisms of NO_x removal by carbon-based catalysts [15–20]. Among the transition metals, iron embedded in a carbon matrix has been identified to be one of the most promising candidates [21,22]. However, catalyzed gasification of the carbon at elevated temperatures is still one of the greatest concerns [23]. Hence, lowering the working temperature at satisfying catalyst performance is a scientifically difficult challenge of technological relevance.

In the present paper we investigate for the first time the NO_x uptake and conversion of iron nanoparticles stabilized in carbon (nano-Fe/C). The catalyst seems suitable for especially low temperature application in order to prevent catalyst consumption. The synthesized material is investigated by scanning transmission electron microscopy (STEM), thermal gravimetric analysis (TGA), differential thermal analysis (DTA) and low temperature nitrogen adsorption. The catalytic conversion of NO_2 is analyzed in recycle

Abbreviations: AC, activated carbon; BJH, Barrett–Joyner–Halenda method; DTA, differential thermal analysis; IWM, incipient wetness method; Nano-Fe/C, iron nanoparticles stabilized in carbon matrix; QMS, quadrupole mass spectrometer; S, catalytically active site; STEM, scanning transmission electron microscope; TGA, thermal gravimetric analysis.

* Corresponding author at: Nanoparticle Process Technology, Faculty of Engineering, University of Duisburg-Essen, Lotharstrasse 1, 47057 Duisburg, Germany.
Tel.: +49 203 379 4446; fax: +49 203 379 4453.
E-mail address: markus.winterer@uni-due.de (M. Winterer).

http://dx.doi.org/10.1016/j.apcatb.2014.11.013
0926-3373/© 2014 Published by Elsevier B.V.

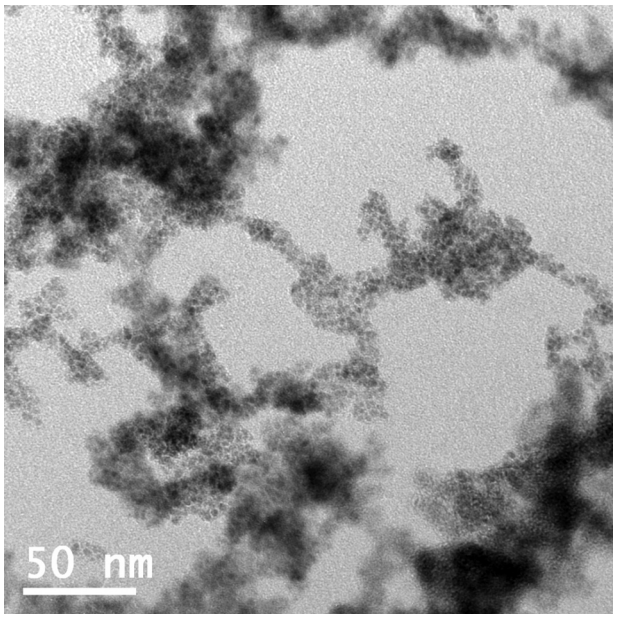

Fig. 1. TEM micrograph showing nano-Fe/C; dark iron particles are visible in the brighter carbon matrix.

flow at 423 K and 328 K. The results are compared to pure and iron-infiltrated activated carbon and to magnetite powder.

2. Experimental methodology

The synthesis of the novel nano-Fe/C material in a chemical vapor synthesis process has been described elsewhere [24,25]. Iron-III-acetylacetonate (99%, ABCR GmbH & Co., KG, CAS: 14024-18-1) serves as organometallic precursor and is evaporated in a flash evaporator, diluted in 2000 sccm helium gas flow [26]. The reactor temperature is 1373 K and the pressure is kept constant at 20 mbar. The powder is collected using thermophoresis. The sample structure is stable at ambient conditions. A TEM micrograph of the agglomerated particles of nano-Fe/C (Fig. 1) is acquired at 200 kV using a Tecnai F20 G^2 transmission electron microscope. Small iron particles are visible as dark spots in contrast to the surrounding opaque carbon matrix.

The material has a specific surface area of (256 m^2/g) as investigated by nitrogen adsorption at 77 K (Quantachrome Autosorb 1C) using the BET method. The pore size distribution is derived from the BJH method. Prior to the measurement, samples are degassed at 423 K for 20 h. The NO_x uptake is analyzed in a thermal balance instrument (Bähr Thermoanalyse GmbH, STA 503) exposing 10 mg of the sample to 0.3% NO_2 in helium at 10 sccm total gas flow with parallel recording of the DTA signal.

Powder X-ray diffractograms of the nano-Fe/C particles before and after exposure to NO_2 in the recycle flow reactor were collected on a PANalytical X'pert Pro MPD using Cu-Kα radiation and a diffracted beam graphite monochromator.

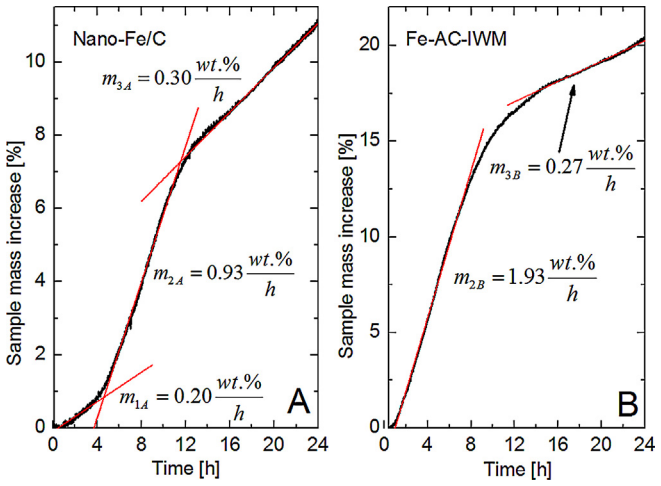

Fig. 3. NO_2 adsorption on nano-Fe/C (A) and Fe-AC-IWM (B) at 297 K.

The catalytic conversion of NO_2 is investigated in a recycle flow reactor described elsewhere [27]. A test gas mixture (0.9 mol% NO_2, 10 mol% Ar, 89.1 mol% He) at ambient pressure is monitored using time–temperature-resolved mass spectrometry (QMS). For calculation of the gas mole fractions the QMS signal at characteristic peaks is normalized to the $m/e = 40$ signal (Ar) in order to avoid pressure-induced artifacts. In the diagrams displaying 120 min experiment time (Figs. 5 and 6), each data point shows the mean of six successive ion signal measurements within 60 s time. A reference measurement with an empty reactor is performed for correction of any signal effect due to leakage. The normalized spectra are fitted with spectra of previously calibrated gases by means of Microsoft Excel Solver 2010. Test measurements with defined gas mixtures ensure the validity of our measurements to a good certainty reflected in the stated error bars. A higher initial concentration of NO_2 was chosen for the mass spectrometric experiments in order to ensure a high dynamic measurement range with small uncertainties.

The NO_x conversion properties of nano-Fe/C are compared to a commercial ball-shaped activated carbon (Rütgers/CarboTech R1407, 1604 m^2/g surface area, denoted as "original AC"), to an iron infiltrated activated carbon (Rütgers/CarboTech R1407, infiltrated with 1-molar iron nitrate solution using the incipient wetness method, provided by Max-Planck-Institute for carbon research in Mühlheim a.d.R., 5 wt.% iron load, 1714 m^2/g surface area, denoted as "Fe-AC-IWM") and to pure magnetite powder (Iron-II,III-oxide, black (magnetite), min. 95%, STREM Chemicals, CAS: 1317-61-9, surface area: 8.4 m^2/g).

3. Results

A comparison of the gas composition with four different catalysts after the entire catalysis experiment time is shown in Fig. 2. Original AC converts NO_2 into NO and desorbs some CO. Fe-AC-IWM converts NO and releases a large amount of N_2O and CO. At the end

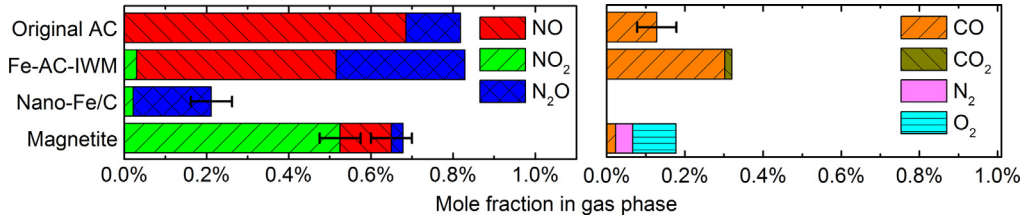

Fig. 2. Gas species mole fractions after 120 min of isothermal NO_2 conversion in recycle flow at 425 K.

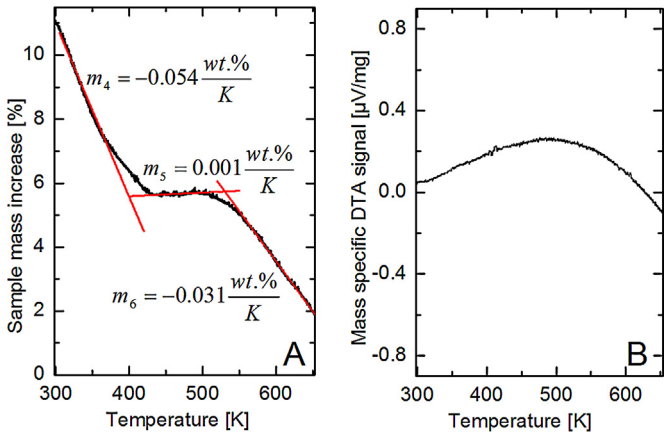

Fig. 4. Mass loss of NO_2-preloaded nano-Fe/C during heating (A) and corresponding DTA signal (B).

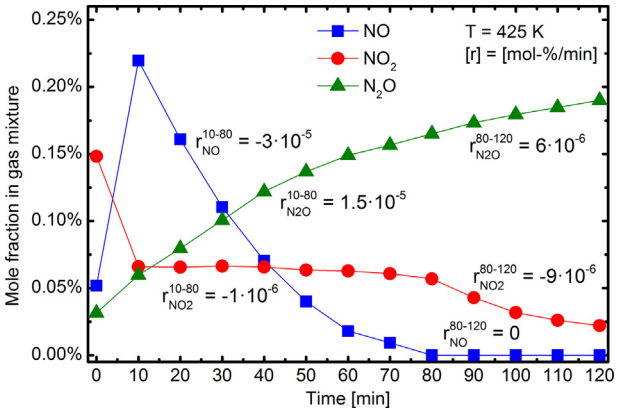

Fig. 5. Composition of the gas mixture during NO_2 conversion by nano-Fe/C at 425 K given as mole fractions; adsorption and desorption rates are stated for the gas species stated in the lower index and for a time interval stated in the upper index.

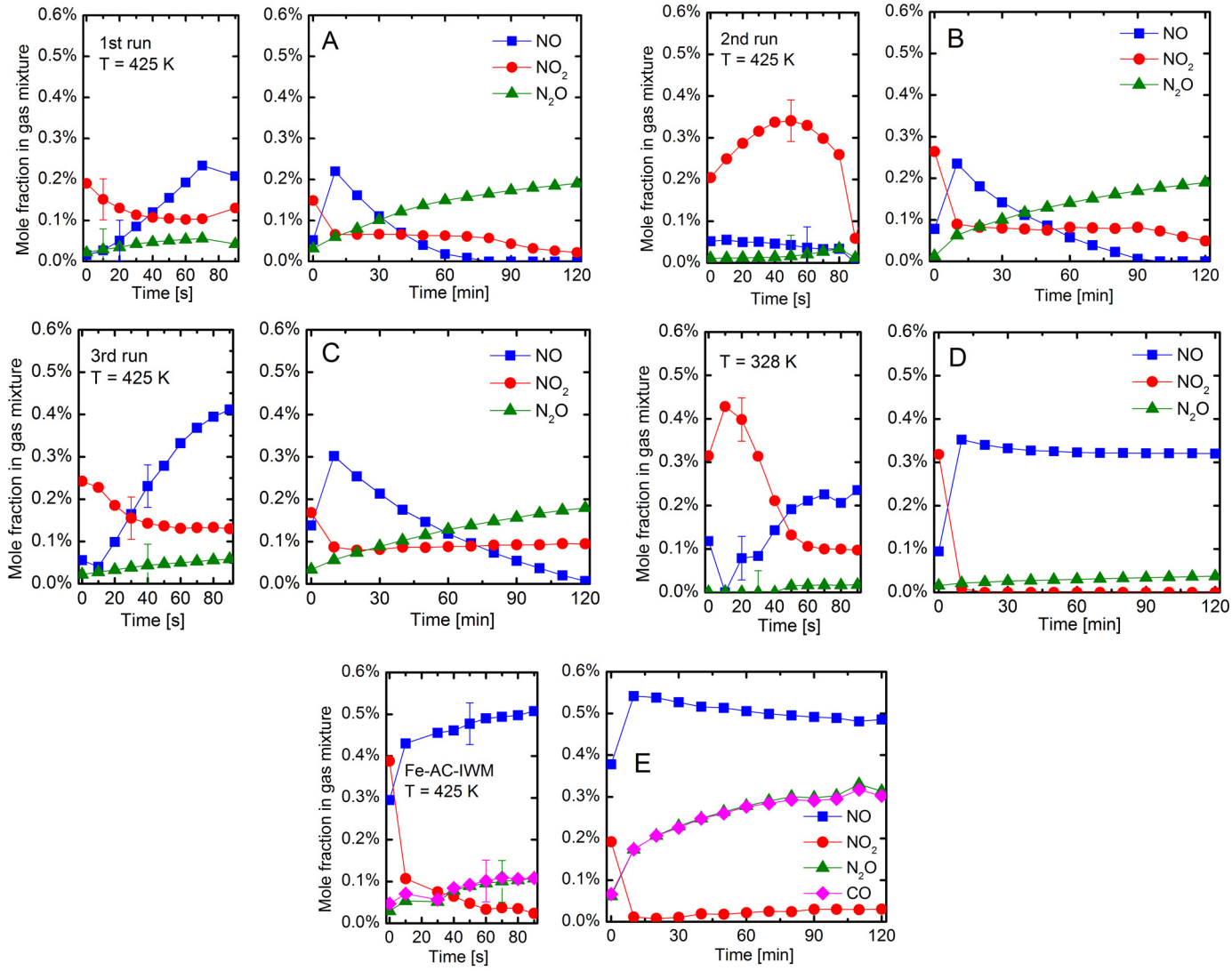

Fig. 6. Gas species mole fractions during isothermal NO_2 conversion in recycle flow for nano-Fe/C in three consecutive runs at 425 K (A–C), at 328 K (D) and iron-infiltrated activated carbon at 425 K (E); the left graphs show the first 90 s of the experiment, the right graphs show the entire experimental time of 120 min; stated error bars are exemplary.

of the experiment some CO_2 emerges. Magnetite adsorbs half of the initial mole fraction of NO_2, but hardly converts NO_2 into NO or N_2O. However, small fractions of O_2 and N_2 are observed. Nano-Fe/C exhibits the largest NO_x-adsorption and only a significant release of N_2O.

NO_2 is adsorbed on nano-Fe/C at room temperature (297 K) in three stages (Fig. 3A). During the first 4 h the average adsorption rate is 0.20 wt.%/h. In the subsequent 8 h the adsorption rate becomes almost five times larger and finally declines to 0.30 wt.%/h during the last 12 h of the experiment. In direct comparison, Fe-AC-IWM (Fig. 3B) exhibits only two stages of adsorption. A large adsorption rate of 1.93 wt.%/h is observed during the first 10 h, decreasing to 0.27 wt.%/h in the remaining experimental time.

Subsequent to NO_x adsorption the preloaded sample is heated from 297 K to 660 K with a heating rate of 3 K/min. The observed desorption or mass loss process exhibits three stages (Fig. 4A), too. The first stage starts at room temperature up to 425 K. Between 425 K and 510 K no further mass loss is detected. Above this temperature the mass loss rate is again uniform up to the final temperature of 650 K. The corresponding DTA signal does not show any enthalpy change apart from the difference in heat capacity of the empty reference crucible (Fig. 4B) [28].

Upon exposure of nano-Fe/C to a test gas mixture with 0.9 mol% NO_2 the NO_x conversion properties of the novel material at low temperature are studied. At 425 K (Fig. 5), the NO_2 mole fraction quickly decreases during the initial period of the experiment until an equilibrium mole fraction of about 0.1 mol% NO_2 is reached. The large emerging NO mole fraction at the beginning declines during the first 80 min experimental time. As soon as NO completely vanishes from the gas phase, the residual NO_2 mole fraction starts to decrease and after 120 min NO_2 less than 0.025 mol% is left in the gas phase. The N_2O mole fraction continuously rises over the entire experimental time. The mole fractions of O_2 and N_2 (not shown) remain constant and close to the impurity level. No desorption of CO or CO_2 is observed. The corresponding adsorption and desorption rates are displayed in Fig. 5.

A comparison of consecutive catalysis experiments with nano-Fe/C at 425 K and 328 K and the iron-infiltrated activated carbon reference catalyst (Fe-AC-IWM) are provided in Fig. 6. Fig. 6A–C, shows the evolution of the test gas mixture in three catalysis experiments at 425 K for 120 min with the same nano-Fe/C sample. The first run (Fig. 6A) is analyzed in detail in Fig. 5. After the first run the recycle reactor is evacuated overnight at room temperature. The second run (Fig. 6B) shows very similar results compared to the first run. However, the early adsorption of NO_2 is slightly postponed by about 6 min. Prior to the third run (Fig. 6C) the recycle reactor with the sample is evacuated again overnight at room temperature and additionally for 1 h at 425 K. As the main difference, the NO desorption is elevated to a measured maximum of 0.45 mol% and NO vanishes from the gas phase only at the very end of the experiment time.

At almost room temperature (328 K, Fig. 6D) the kinetics of NO_2 reduction are slower and both the conversion reaction of NO and desorption of N_2O are almost negligible. Anyway, the supplied NO_2 is adsorbed by the sample during the first 10 min of the experiment.

Compared to nano-Fe/C, Fe-AC-IWM (Fig. 6E) exhibits a larger conversion of NO_2 into NO. After the first minute of the experiment the NO mole fraction is decreasing and equimolar amounts of N_2O and CO are desorbed to the atmosphere.

Gasification of carbon in nano-Fe/C during the catalysis experiment would be most probably associated with a significant loss of specific surface area. The specific surface area of originally 256 m^2/g hardly changes during the experiment at 328 K (244 m^2/g after the catalysis experiment) and also the pore size distribution of nano-Fe/C displayed in Fig. 7 changes only marginally.

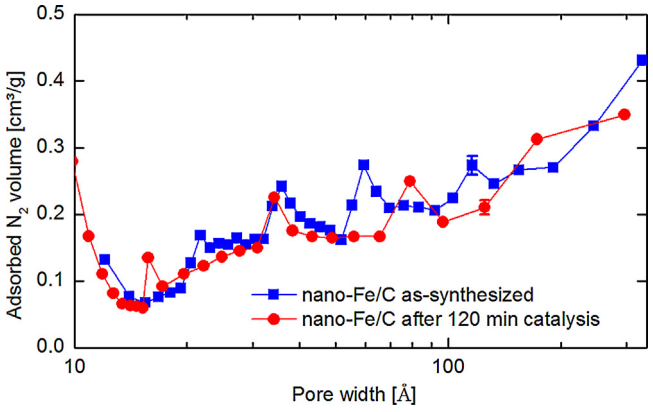

Fig. 7. Pore size distribution of the as-synthesized nano-Fe/C and after the catalysis experiment with NO_2 at 328 K; logarithmic pore width scale.

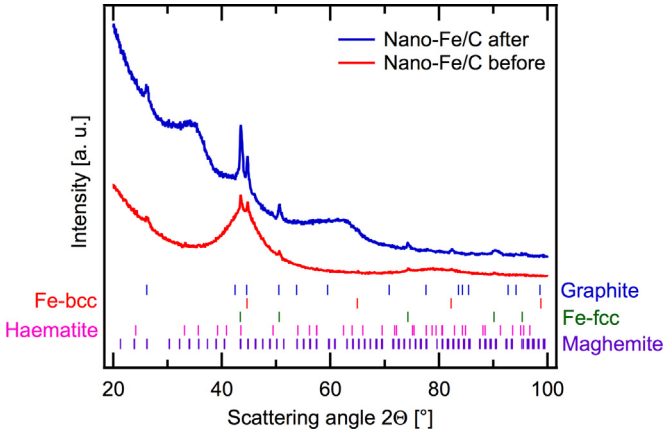

Fig. 8. Powder X-ray diffractogram of the nano-Fe/C particles as synthesized (before exposure to NO_2) and after exposure to NO_2 in the recycle flow reactor. The tics indicate the calculated positions of Bragg reflections from each phase listed.

In the X-ray diffractogram (Fig. 8) reflections of very small and larger nanometer sized iron particles in bcc and fcc structure are observed as well as a single reflection peak that can be attributed to graphite. The high background at low scattering angles is due to the tail of small angle scattering caused by the very small particles.

Structural changes are observed in the nano-Fe/C powder after being used for NO_2 conversion in the recycle flow reactor. The two dominant reflection peaks from bcc and fcc iron become more pronounced as the broad peak underneath, probably from very small iron particles, diminishes. Additionally, two broad peaks arise between 25° and 35° 2θ and 55–65° 2θ. The strongest reflections are due to α-Fe_2O_3 (haematite) and γ-Fe_2O_3 (Maghemite) probably due to the formation of very small iron oxide clusters.

4. Discussion

4.1. NO_2 adsorption behavior

The first stage of NO_2 adsorption in nano-Fe/C (Fig. 3) is probably dominated by NO_2 physisorption on the carbon shell [29], which is encapsulating the iron particles. Chemisorption on the carbon surface reportedly requires substantial activation energy [30] and is, therefore, rather unlikely at room temperature. No effects that would be expected from the adsorption enthalpy of chemisorption are found in the corresponding DTA signal (not shown). Still, some NO_2 could be slowly reduced to desorbing NO, leaving behind an oxidized surface [31]. The low mass gain contribution of the single

oxygen atom in comparison to physisorbed NO_2 could explain the slow mass increase in the first 4 h adsorption time.

In the second stage after about 4 h the carbon surface might be fully oxidized and NO_2 molecules could entirely physisorb. As soon as the easily accessible sites of the material are saturated with NO_2 – after about 12 h experiment time – NO_x species might diffuse along cracks, grain boundaries or pore channels into the carbon matrix and to the iron. This stage of adsorption is characterized by a lower net mass gain since the kinetics of the diffusion process is probably slower than physisorption on easily accessible sites.

In Fe-AC-IWM right from the beginning NO_2 can be adsorbed in micropores and accessible iron clusters. The seven times larger specific surface area can cause the observed large adsorption rate, which is probably mass transfer controlled. Probably after micropore filling the adsorption rate decreases.

The first stage of desorption (Fig. 4) is characterized by a possible release of adsorbed NO_x species. At 420 K NO_x may become scarce on the sample [32] and above 520 K reportedly the decomposition of oxidic surface complexes and desorption of CO or CO_2 starts [13,16].

4.2. Conversion of NO_x and catalyst aging

Several mechanisms describing the observed NO_x conversion behavior are proposed in the literature. According to [16], an initial fast adsorption of NO_2 on the catalyst surface can be accompanied with chemisorption, reduction to NO and oxidation of the catalyst surface:

$$NO_2 + S^* \rightarrow S(NO)_2, \quad (1)$$

where "S" denotes an active iron or carbon surface site

$$S(NO_2) \leftrightarrow S(O) + NO \quad (2)$$

$$S(O) + NO_2 \rightarrow S(ONO_2) \quad (3)$$

The desorption of NO according to equilibrium reaction (2) is supposed to be kinetically much faster than a possible subsequent conversion of NO into N_2O. Significant formation of N_2O, as observed in our catalysis experiments, has not been reported or has been neglected in previous studies [15–18]. Some authors [22,33] suggest the formation of N_2O in connection with a dissociative chemisorption of NO_2 or NO:

$$NO + 2S^* \rightarrow S(O) + S(N) \quad (4)$$

$$S(N) + NO \rightarrow S^* + N_2O \quad (5)$$

In the present experiments this mechanism seems unlikely, since the presence of S(N) and S(O) would be associated with desorption of N_2 and CO_2 [34] which is not observed in the experiments with nano-Fe/C.

Alternatively, Okuhara and Tanaka describe the desorption of N_2O from NO as [34]:

$$2NO + S^* \rightarrow S(NO)_2 \quad (6)$$

$$S(NO)_2 \rightarrow N_2O + S(O) \quad (7)$$

Reaction (6) – as well as reaction (4) – would require available active sites. Since the adsorption of the remaining NO_2 in the test gas would be energetically preferred to the adsorption of NO at the regarded temperature [35], there is probably a selective adsorption of NO. Hence, the NO_2 mole fraction remains constant at 0.1 mol%, until NO disappears completely from the gas phase.

With the oxidized catalyst surface and predominantly NO in the gas mixture after reaction (2) N_2O might be formed in an Eley-Rideal-type process:

$$S(O) + NO \rightarrow S(NO_2), \quad (8)$$

as proposed e.g. by [36]

$$S(NO_2) + NO \rightarrow N_2O + S(O_2) \quad (9)$$

According to this scheme the consumption of NO is twice as large as the desorption of N_2O which is in good accordance with our observations between the 10th and 80th min (see Fig. 5).

As soon as NO disappears from the gas phase after about 80 min, the release of N_2O is accompanied with almost equimolar decrease of NO_2 without any intermediate NO release to the gas phase. Hence, NO_2 could possibly adsorb on primary N_2O-formation sites from reaction (8):

$$2S(NO_2) \rightarrow N_2O + S(O) + S(O_2) \quad (10)$$

$$S(O) + NO_2 \rightarrow S(ONO_2)$$

Reaction (10) probably carries on as long as the reaction product $S(NO_2)$ from reaction (8) is available on the surface. Eventually, the surface might be mainly covered with the $S(ONO_2)$ surface complexes and some $S(O_2)$. The latter could finally lead to desorption of molecular oxygen, which is, however, in the current experiments only detected for the magnetite reference catalyst.

For a carbon-based catalyst the thermal decomposition of the surface complexes including $C(ONO_2)$ would be associated with release of CO and CO_2 [16] which is also not observed. Probably, the activation energy for CO and CO_2 release is not sufficient during the catalysis experiments.

The second and the third run of the experiment show that the catalyst is fully recoverable after evacuation. An additional thermal treatment prior to the third run even seems to increase the NO_2 reduction and NO release. Close to room temperature (328 K) the catalyst surface seems to be deactivated for further NO decomposition after reduction of NO_2 into NO.

For Fe-AC-IWM the parallel release of N_2O and CO may indicate a connected mechanism involving adsorbed NO_2 on iron (denoted as "M"), in addition to the above discussed possible NO_2 reduction on carbon sites:

$$M^* + NO_2 \rightarrow M(O) + NO \quad (11)$$

$$M(O) + C^* \rightarrow M^* + C(O) \quad (12)$$

oxygen transfer from the metal to the carbon matrix

$$C^* + NO_2 \rightarrow C(NO_2) \quad (13)$$

$$C(NO_2) + C^* \rightarrow C(NO) + C(O) \quad (14)$$

whereas reactions (14) and (15) reportedly occur preferentially in small carbon micropores [18,37,38]. Reaction (15) could be followed by a release of N_2O from neighboring C–NO complexes:

$$2C(NO) \rightarrow N_2O + C(O) + C^* \quad (15)$$

$$C(O) \rightarrow CO \quad (16)$$

or alternatively by the N_2O release after C-NO dissociation:

$$C(NO) + C^* \rightarrow C(N) + C(O) \quad (17)$$

$$C(N) + C(NO) \rightarrow N_2O + C^* \quad (18)$$

$$C(O) \rightarrow CO \quad (19)$$

The former alternative is probably more likely in the present experiment, since reaction (17) would be associated with a release of some N_2 from neighboring C—N [34], which is not observed.

In contrast to nano-Fe/C, the Fe-AC-IWM releases a substantial amount of CO, probably associated to the availability of unsaturated carbon atoms on its surface [39]. The initial large conversion of NO_2 into NO of Fe-AC-IWM may be caused by a good availability of NO_2 chemisorption sites in the activated carbon material. Additionally,

the large specific surface area of micropores and the well accessible catalytic iron sites could contribute to the effect.

The subsequent conversion of the product N_2O by carbon-based catalysts is subject of other studies [40,41] and needs to be further investigated in detail. However, this product gas is by far less toxic than the original nitrogen oxides [42,43].

X-ray diffraction shows that the very small iron particles almost vanished after the catalytic process and may have merged to form larger crystallites, most likely during heating to 650 K before the recycle flow investigation. During the catalytic process the iron particles partially oxidize, probably forming small haematite or maghemite nanoparticles.

5. Conclusions

In the present work we investigate the properties of uptake and conversion of NO_x by iron nanoparticles stabilized in carbon. The adsorption of NO_2 at 297 K reveals to be a three-step-process. Initially NO_2 is probably reduced to NO in the carbon shell. Subsequently NO_2 may weakly physisorb and finally NO_x species may diffuse in the carbon matrix and possibly to the iron nanoparticles.

During investigation of the NO_x catalysis in recycle flow at 425 K, NO_2 is quickly reduced to NO and N_2O is subsequently released upon NO conversion. As soon as NO completely vanishes from the gas phase, the residual mole fraction of NO_2 in the test gas is obviously converted to N_2O.

No severe catalyst deactivation or catalyst formation is observed at 425 K. A thermal treatment of the sample even improves the NO_2 reduction behavior. Hence, nano-Fe/C exhibits superior NO_x-removal properties at very low temperature compared with the untreated or iron-infiltrated activated carbon or with a magnetite reference catalyst. Even at room temperature nano-Fe/C still converts the supplied nitrogen oxides, although the product NO is not further converted.

Acknowledgements

The authors thank Mr. A. Görnt for technical support, Professor Michael Farle for his support in the TEM microscopy and Dr. Wolfgang Schmidt of the Max-Planck-Institute für Kohlenforschung (Mülheim an der Ruhr) for kindly providing the reference catalysts. The authors would like to thank for financial support from the German Federal Ministry of Economics and Technology within the agenda for the promotion of industrial cooperative research and development (IGF) based on a decision of the German Bundestag. The access was opened by the IUTA e. V., Duisburg, and organized by the AiF (IGF-Project No. 15751N).

References

[1] E. Jobson, Top. Catal. 28 (2004) 191.
[2] G. Centi, S. Perathoner, Appl. Catal. A: Gen. 132 (1995) 179–259.
[3] H. Bosch, F. Janssen, Catalytic Reduction of Nitrogen Oxides. A Review on the fundamentals and Technology, Elsevier, 1988, VII pp.
[4] R. Burch, J.P. Breen, F.C. Meunier, Appl. Catal. B: Environ. 39 (2002) 283.
[5] R. Burch, P.J. Millington, Catal. Today 26 (1995) 185.
[6] M. Shelef, Chem. Rev. 95 (1995) 209.
[7] S. Roy, M.S. Hegde, G. Madras, Appl. Energy 86 (2009) 2283.
[8] G. Liu, P.-X. Gao, Catal. Sci. Technol. 1 (2011) 552–568.
[9] N. Takahashi, H. Shinjoh, T. Iijima, T. Suzuki, K. Yamazaki, K. Yokota, H. Suzuki, N. Miyoshi, S.-I. Matsumoto, T. Tanizawa, T. Tanaka, S.-S. Tateishi, K. Kasahara, Catal. Today 27 (1996) 63.
[10] M.A. Gómez-García, V. Pitchon, A. Kiennemann, Environ. Int. 31 (2005) 445.
[11] M.S. Shah, J. Chem. Soc. (1929) 2676–2692.
[12] M.S. Shah, J. Chem. Soc. (1929) 2661–2676.
[13] J. Zawadzki, M. Wisniewski, K. Skowronska, Carbon 41 (2003) 235–246.
[14] M.S. Akhter, A.R. Chughtai, D.M. Smith, J. Phys. Chem. 88 (1984) 5334–5342.
[15] N. Shirahama, S.H. Moon, K.H. Choi, T. Enjoji, S. Kawano, Y. Korai, M. Tanoura, I. Mochida, Carbon 40 (2002) 2605–2611.
[16] M. Jeguirim, V. Tschamber, J.F. Brilhac, P. Ehrburger, J. Anal. Appl. Pyrol. 72 (2004) 171–181.
[17] W.-J. Zhang, A. Bagreev, F. Rasouli, Ind. Eng. Chem. Res. 47 (2008) 4358–4362.
[18] X. Gao, S. Liu, Y. Zhang, Z. Luo, M. Ni, K. Cen, Fuel Process. Technol. 92 (2011) 139–146.
[19] B. Azambre, S. Collura, J.M. Trichard, J.V. Weber, Appl. Surf. Sci. 253 (2006) 2296–2303.
[20] H. Muckenhuber, H. Grothe, Carbon 44 (2006) 546–559.
[21] S. Bashkova, T.J. Bandosz, ChemSusChem 4 (2011) 404–412.
[22] M.J. Illán-Gómez, A. Linares-Solano, L.R. Radovic, C. Salinas-Martínez de Lecea, Energy Fuels 10 (1996) 158–168.
[23] M.J. Illán-Gómez, E. Raymundo-Pinero, A. García-García, A. Linares-Solano, C. Salinas-Martínez de Lecea, Appl. Catal. B: Environ. 20 (1999) 267–275.
[24] M. Winterer, Nanocrystalline Ceramics: Synthesis and Structure, Springer Verlag, Berlin, 2002.
[25] T. Enz, M. Winterer, B. Stahl, S. Bhattacharya, G. Miehe, K. Foster, C. Fasel, H. Hahn, J. Appl. Phys. 99 (2006) 044306.
[26] M. Winterer, V.V. Srdic, R. Djenadic, A. Kompch, T.E. Weirich, Rev. Sci. Instrum. 78 (2007) 123903–123905.
[27] M. Busch, U. Bergmann, U. Sager, W. Schmidt, F. Schmidt, C. Notthoff, B. Atakan, M. Winterer, J. Nanosci. Nanotechnol. 11 (2011) 7956–7961.
[28] J. Yang, C. Roy, Thermochim. Acta 333 (1999) 131–140.
[29] H. Teng, E.M. Suuberg, J. Phys. Chem. 97 (1993) 478–483.
[30] W.-L. Yim, X.G. Gong, Z.-F. Liu, J. Phys. Chem. B 107 (2003) 9363–9369.
[31] H. Teng, E.M. Suuberg, Ind. Eng. Chem. Res. 32 (1993) 416–423.
[32] A.M. Rubel, M.L. Stewart, J.M. Stencel, J. Mater. Res. 10 (1995) 562–567.
[33] H. Teng, E.M. Suuberg, J.M. Calo, Energy Fuels 6 (1992) 398–406.
[34] T. Okuhara, K.-I. Tanaka, J. Chem. Soc. Faraday Trans. 1: Phys. Chem. Condens. Phases 82 (1986) 3657–3666.
[35] J.K. Neathery, A.M. Rubel, J.M. Stencel, Carbon 35 (1997) 1321.
[36] E. Richter, H.-J. Schmidt, H.-G. Schecker, Chem. Eng. Technol. 3 (1990) 332–340.
[37] K. Kaneko, Langmuir 3 (1987) 357–363.
[38] A.M. Rubel, M.L. Stewart, J.M. Stencel, Reduction of Nitrogen Oxide Emissions, American Chemical Society, 1995, pp. 208–216.
[39] B. Xia, J. Phillips, C.-K. Chen, L.R. Radovic, I.F. Silva, J.A. Menendez, Energy Fuels 13 (1999) 903–906.
[40] S.A. Carabineiro, F.B. Fernandes, R.J.C. Silva, J.S. Vital, A.M. Ramos, I.M. Fonseca, Catal. Today 133–135 (2008) 441–447.
[41] J.A.Z. Pieterse, S. Booneveld, R.W. van den Brink, Appl. Catal. B: Environ. 51 (2004) 215–228.
[42] WHO, WHO Guidelines for Indoor Air Quality: Selected Pollutants, World Health Organization, Bonn, 2010.
[43] BAuA, Technische Regeln für Gefahrstoffe, TRGS 900, in: Bundesanstalt für Arbeitsschutz und Arbeitmedizin – Ausschuss für Gefahrstoffe (Ed.), Arbeitsplatzgrenzwerte, Januar 2006.